FLUCOME 2009
10th International Conference on Fluid Control, Measurements, and Visualization
August 17–21, 2009, Moscow, Russia

EFFECT OF CORNER CUTOFFS ON FLOW CHARACTERISTICS AROUND A SQUARE CYLINDER

Yoichi Yamagishi[1], Shigeo Kimura[1], Makoto Oki[2] and Chisa Hatayama[3]

ABSTRACT

It is known that for a square cylinder subjected to uniform flow, the drag force changes with the shape of corner cutoffs. To clarify the flow characteristics around a square cylinder with corner cutoffs we measured the drag coefficient and the Strouhal number for changing chamfer shape and dimensions. We analyzed the flow around a square cylinder with corner cutoffs by applying the RNG k–ε turbulent model, and investigated the surface flow pattern using visualization by means of the oil-film and mist flow method. From these results, we obtained the surface flow patterns by the oil-film method and numerical analysis. The drag coefficient of the square cylinder with corner cutoffs decreased suddenly at an angle of attack of about α = 0~10° when compared with the drag coefficient for a square cylinder. The minimum value of the drag coefficient for the square cylinder with corner cutoffs decreased by about 30 % compared with that for the square cylinder. The drag coefficient of the square cylinder with 10% corner cutoffs was found to be smallest, since the wake area of this square cylinder was smaller compared with that of the other square cylinder.

Keywords: Square Cylinder, Corner Cutoffs, Drag coefficient, Flow visualization, Numerical Analysis.

INTRODUCTION

It is known that the maximum value of the drag coefficient of a square cylinder is about 2 at zero angle of attack, but that of a circular cylinder is about 1.2, and the drag coefficient of a square cylinder increases by about 60 % compared with that of a circular cylinder. There are many structures with square cylinder shapes, such as high-rise buildings, to which we can apply the theoretical study of drag reduction of a square cylinder to reduce wake flow and wind load. A square cylinder was examined experimentally (Igarashi, 1984; Shao et al., 2007). A square cylinder with grooves and tabs was examined (Koide et al., 2006; Layukallo et al., 2003; Yamagishi et al., 2004). A square cylinder with rectangular cutouts at its edges was examined experimentally (Kurata et al., 1998). However, there has been no complete investigation into the effect of corner cutoffs on the flow characteristics around a square cylinder.

In this study, we examined the flow characteristics around a square cylinder with corner cutoffs for

[1] Department of Mechanical Engineering, Kanagawa Institute of Technology
[2] Corresponding author: School of High-Technology for Human Welfare, Tokai University, e-mail:oki@wing.ncc.u-tokai.ac.jp
[3] Graduate School of High-Technology for Human Welfare, Tokai University

changing chamfer shape, dimensions and angles of attack by using experiments, numerical analysis, and visualization.

EXPERIMENTAL METHOD AND NUMERICAL ANALYSIS

Experimental Apparatus

Figure 1(1) shows the square cylinder with corner cutoffs used for this experiment. The cylinder was made of aluminum and was 420 mm in length with 30 × 30 mm cross-sectional dimensions *d*. Fig. 1(2) shows the square cylinder with rectangular and arc corner cutoff were used for this experiment. In addition, the square cylinder with straight corner as C1, C3, and C5 cylinders that have chamfers with lateral dimensions of 1, 3 and 5 mm cut along the corners of each square cylinder as shown in Fig. 1(3) were used.

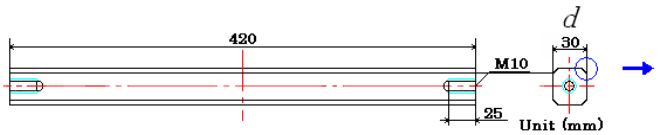

(1) Whole test cylinder.

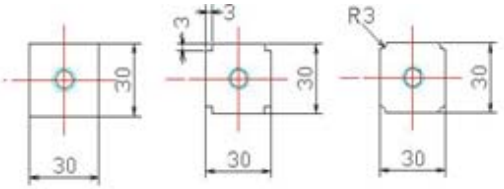

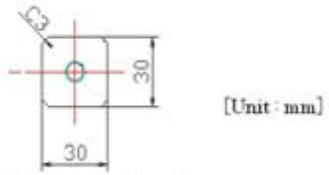

(2) Shape of chamfer.

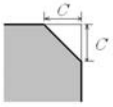

Type	Cutoff length C(mm)	C/d
Square cylinder	0	0
C1	1	0.033
C3	3	0.1
C5	5	0.167

(3) Changing chamfer dimension of straight type.

Fig. 1. Test cylinders.

Figure 2 shows the schematic diagram for the experimental apparatus. We conducted the experiments in a 400 mm × 400 mm circulating wind tunnel with a turbulence intensity of about 0.65% and a maximum speed of around 35 m/s. We placed the cylinder vertically in the measuring section of the wind tunnel. The flow around the cylinder was examined for Reynolds numbers $Re = Ud/\nu$ (d is the side length of the cross section of the cylinder, U is the uniform flow velocity, ν is the kinematic viscosity) ranging from 1×10^3 to 6×10^4.

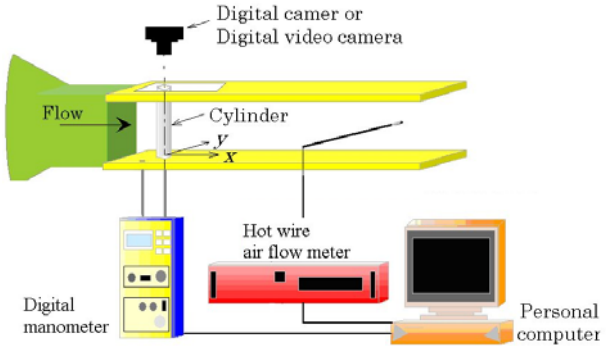

Fig. 2. Experimental apparatus and instruments.

Measurement and Visualization

We obtained the drag from the change in momentum in front of and behind the cylinder. Measurements of the velocity were made using an IHW hot-wire anemometer (sampling time: 1 ms) by moving the hot-wire probe in the *y*-axis direction. We digitized the output signals on a personal computer. Initially we obtained the drag coefficients C_D of the square cylinder using this drag measurement method. We confirmed that these drag coefficients C_D equaled the drag coefficients of a square cylinder (Lee, 1975; Ohtsuki et al., 1978), and then proceeded to obtain the drag coefficients C_D of the square cylinder with corner cutoffs. We used the IHW to measure the frequency of the generating vortex *f*.

We observed the flow around the cylinder made visible by means of a propylene glycol mixture mist as a tracer. We painted the surface of the cylinder black and covered it with a white oil film dissolved in a solution of titanium oxide composed of liquid paraffin and oleic acid. We took photographs of the cylinder surface and around the cylinder using a digital camera and a video camera.

Numerical Analysis

We performed numerical analysis with the versatile fluid analysis software package, Fluent 6.3, using the finite volume method. The analysis was made in unsteady two-dimensional turbulent flow. The RNG k–ε model was used as a turbulent model. Figure 3 shows a complete view of the mesh and boundary conditions.

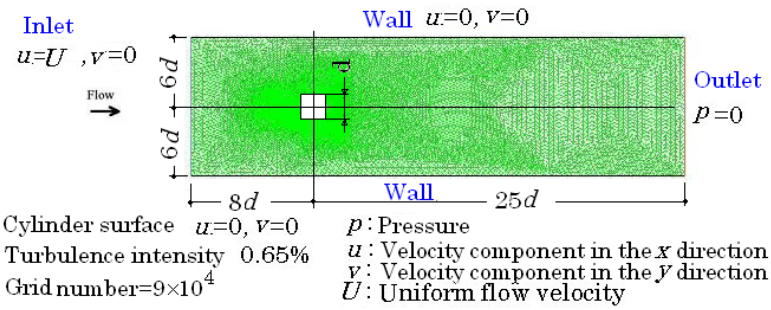

Fig. 3. Whole meshes and boundary conditions.

RESULTS AND DISCUSSION

We obtained the drag coefficient C_D from the drag measurements and numerical analysis.

Figure 4 shows the variations in the drag coefficient C_D by the experiment with Reynolds number for square cylinders with changing chamfer shape shown in Fig. 1(2). In the case of the square cylinder with 10% straight cutoffs (C3 type), the drag coefficient is less than that in the case of the other cutoffs.

Figure 5 shows the computational results of the streamlines around the square cylinder for changing chamfer shape. It is clear that the value of the drag coefficient C_D will become small as separation area becomes small. The C3 cylinder is the smallest value of drag coefficient and separation area.

Furthermore, we investigate in detail about the square cylinder with straight cutoffs shown in Fig. 1(3).

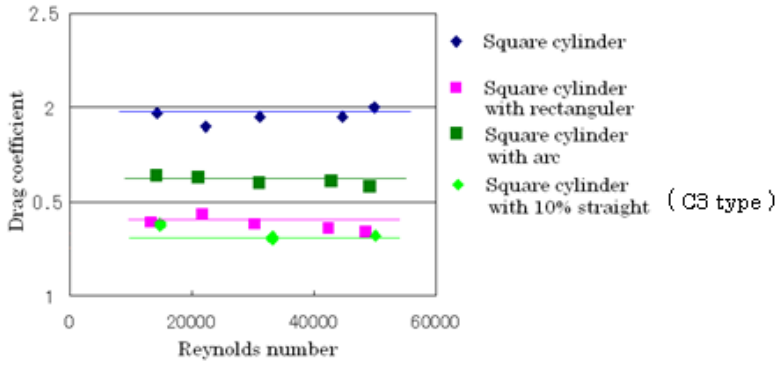

Fig. 4. Drag coefficient for changing chamfer shape by the experiment.

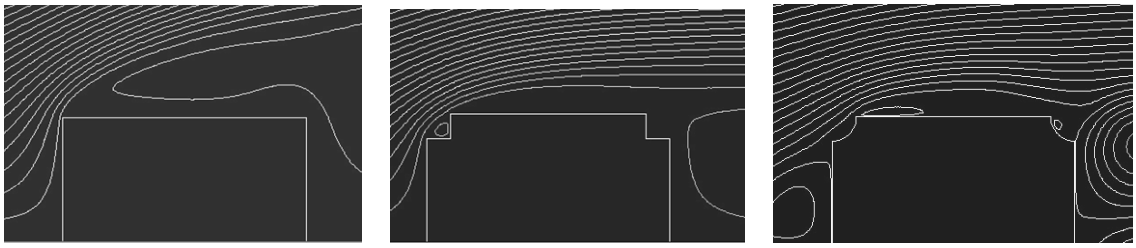

(a) Square **(b) Rectangular** **(c) Arc**

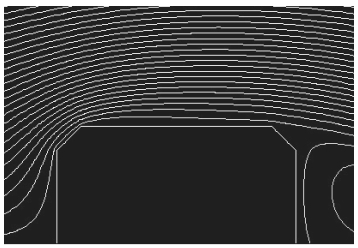

(d) Straight(10%) : C3 type

Fig. 5. The computational results of the streamlines for changing chamfer shape.

Figure 6 shows the variations in the drag coefficients C_D with the angle of attack α for cylinders. Right-hand side is an enlarged figure. The measurement on a square cylinder (Lee, 1975; Ohtsuki et al., 1978) is also included for comparison. The drag coefficient C_D of C1 cylinder is the almost same value as the square cylinder. The sudden decrease of the drag coefficients C_D occurs at about α = 0~10° in the case of the C3 and C5 cylinders compared with the square cylinder. Further, the drag coefficients C_D of C3 cylinder is less than that of C5 cylinder. The minimum value of the drag coefficient C_D for the C3 cylinder decreases by about 30% compared with that for the square cylinder. The results of the numerical analysis show a tendency to agree well with the experimental values.

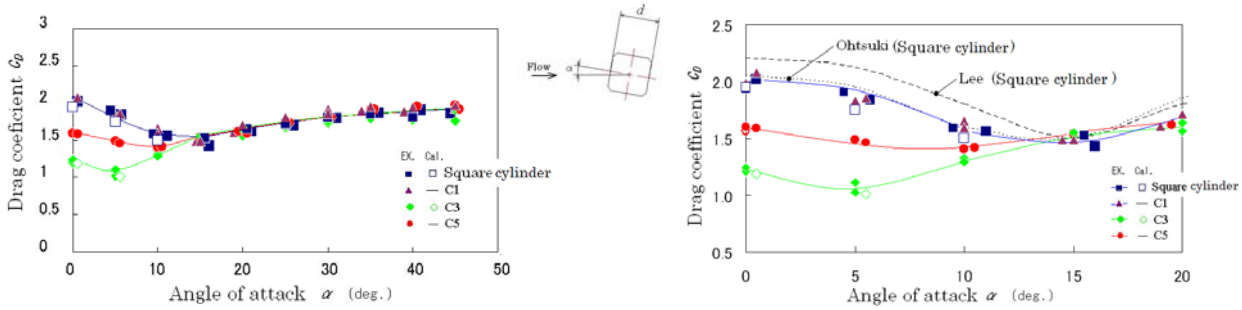

Fig. 6. Drag coefficient of square cylinders with corner cutoffs and square cylinder.

Figure 7 shows the variations of the drag coefficients C_D with the chamfer dimension C for four kinds of cylinders at $\alpha = 0°$ for $Re = 6 \times 10^4$. The value of the drag coefficients C_D of each cylinder is a constant value of about 2 in the range of $C/d = 0$ (Square cylinder) ~ 0.033 (C1 cylinder), then falls abruptly to a minimum value of about 1.2 at $C/d = 0.1$ (C3 cylinder), and then increases slightly.

Figure 8 shows the flow patterns around the square, C3 and C5 cylinders, which were made visible by using the propylene glycol mixture mist flow at $\alpha = 0°$ for $Re = 1 \times 10^3$.

Figure 9 shows the computational results of the streamlines around the square, C3 and C5 cylinders. The flow patterns obtained using the mist flow and numerical analysis methods agree well.

In the separation areas of the side face of a square cylinder and square cylinder with cutoffs, the area of C3 cylinder is small compared with the square and C5 cylinders.

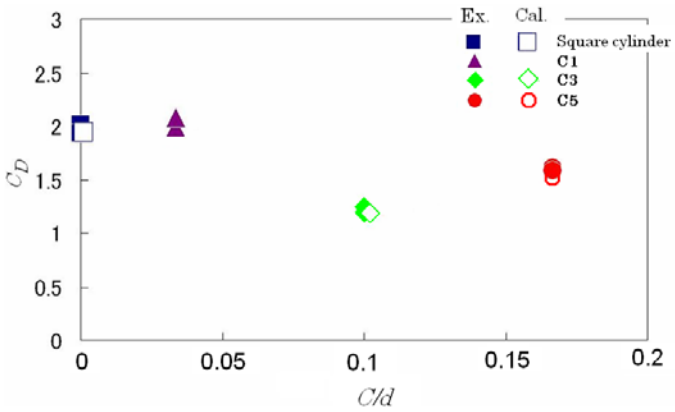

Fig. 7. Drag coefficient of cylinders at $\alpha = 0°$.

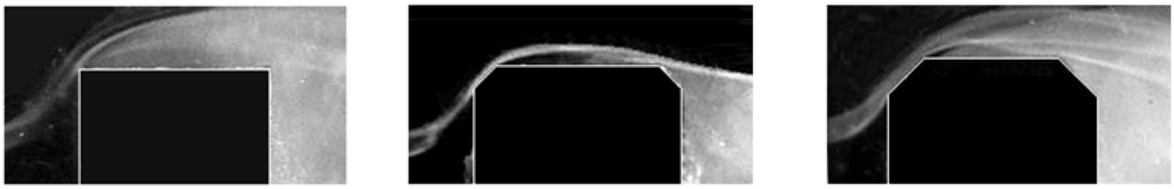

(a) Square cylinder **(b) C3 cylinder** **(c) C5 cylinder**

Fig. 8. The flow patterns around the cylinder which were visualized by using the propylene glycol mixture mist flow.

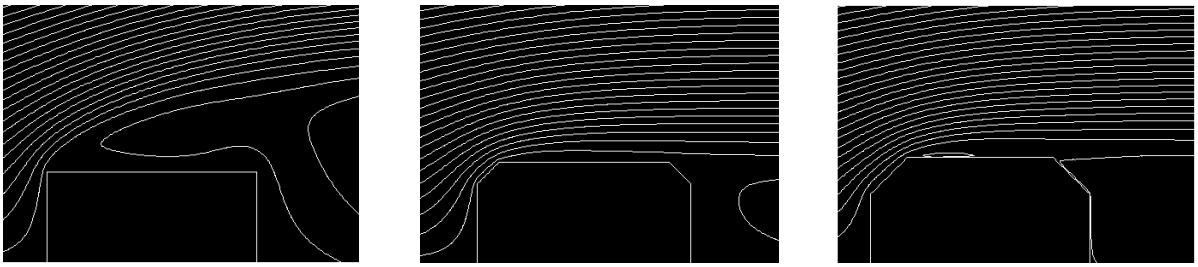

(a) Square cylinder **(b) C3 cylinder** **(c) C5 cylinder**

Fig. 9. The computational results of the streamlines around the cylinder.

Figures 10 shows the flow patterns along the square, C3 and C5 cylinder surfaces that were made visible using the white oil film method at α = 0° for $Re = 6 \times 10^4$. In addition, Fig. 11 shows the shear stress by numerical analysis at the D corner.

Both the A and D corners of the square cylinders with corner cutoffs show peeling of the white oil film by forward flow. Peeling of a white oil film is the black portion shown by the red arrows. The

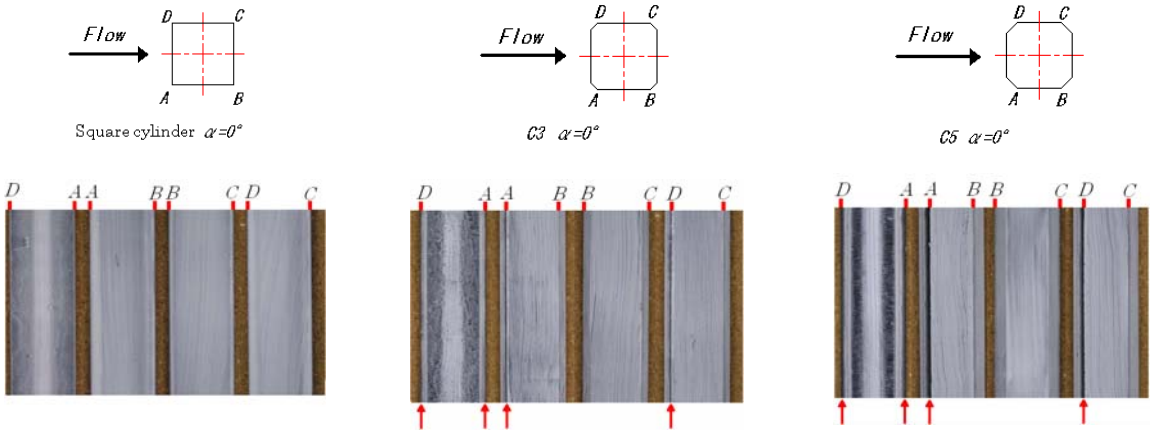

(a) Square cylinder **(b) C3 cylinder** **(c) C5 cylinder**

Fig. 10. Oil-pattern along the cylinders.

peeling area of the white oil film of C5 cylinder is large compared with that of C3 cylinder, and the shear stress is large.

We checked the shear stress by numerical analysis. Large value of the shear stress of C5 cylinder is red. We also noted that the tangential velocity of the corner end side of C5 cylinder becomes large compared with C3 cylinder, and enlarges the separation area of the cylinder side face.

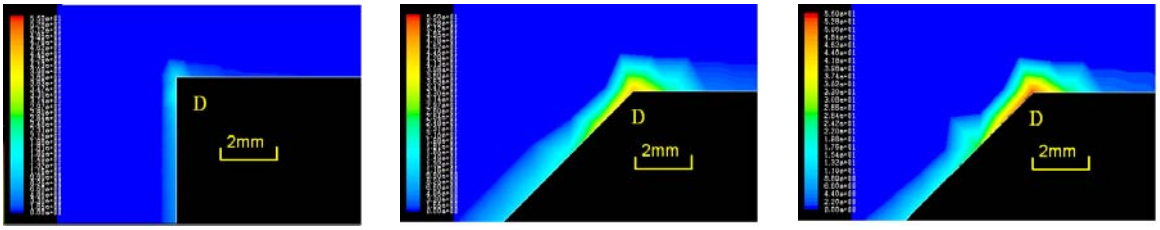

(a) Square cylinder **(b) C3 cylinder** **(c) C5 cylinder**

Fig. 11. The computational results of the shear stress around the cylinder.

The computational results of the velocity distributions at the front face of the cylinder to the 0.3d position on the cylinder side surface at $Re = 6 \times 10^4$ are shown in Fig. 12. The ordinate shows y/d (y is the distance from the center of the cylinder to the measurement position, d is the width of the cylinder) and the abscissa shows u/U (u is the velocity component in the x direction, U is the uniform velocity). The velocity distribution on the cylinder surface for the C3 cylinder becomes larger compared with the square cylinder and the C5 cylinder.

The experimental results of the velocity distributions u/U at $x/d = 16$ behind the cylinders at $\alpha = 0°$ for $Re = 6 \times 10^4$ are shown in Fig. 13. The velocity of C1 cylinder is the almost same value as the square cylinder. The value of the velocity behind the C3 cylinder at $\alpha = 0°$ becomes large. The large velocity behind the cylinder decreases the drag coefficient.

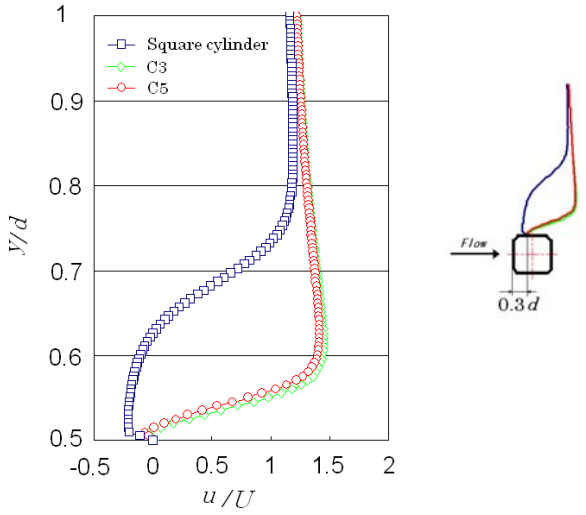

Fig. 12. The computational results of the velocity

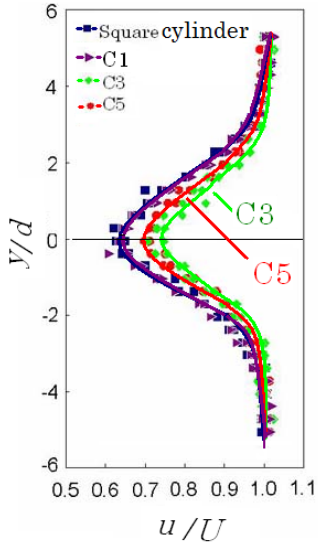

Fig. 13. The experimental results of the velocity

The turbulent kinetic energy k distributions around the square, C3 and C5 cylinders at $\alpha = 0°$ for $Re = 6 \times 10^4$ are shown in Fig. 14. The maximum value of the turbulent kinetic energy around C3 cylinder becomes small compared with that for the square and C5 cylinders.

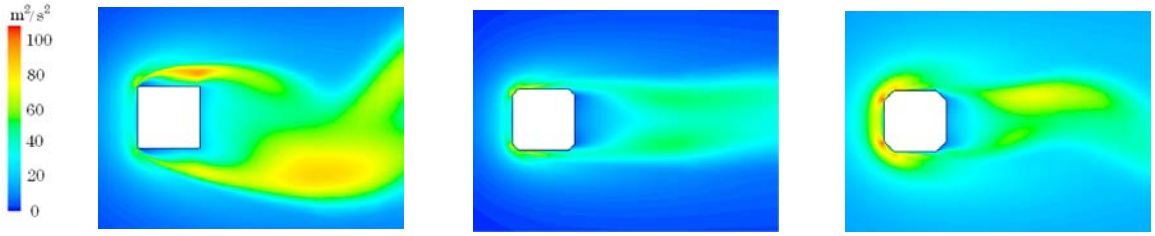

(a) Square cylinder **(b) C3 cylinder** **(c) C5 cylinder**

Fig. 14. The turbulent kinetic energy distributions around the cylinder.

The computational results of the pressure distributions around the square, C3 and C5 cylinders at $\alpha = 0°$ for $Re = 6 \times 10^4$ are shown in Fig. 15. From these results, we observed that the pressure on the downstream side of the cylinder is smaller than that on the upstream side of the cylinder. It is clear that the pressure on the downstream side of the C3 cylinder becomes greater than on the downstream side of the square and C5 cylinders.

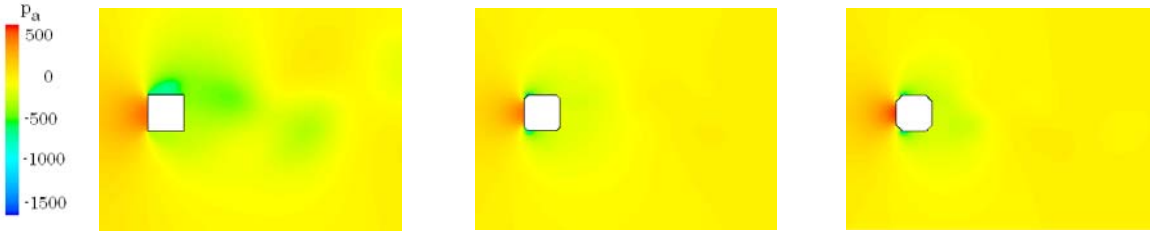

(a) Square cylinder **(b) C3 cylinder** **(c) C5 cylinder**

Fig. 15. The computational results of the pressure distributions around the cylinder

Figure 16 shows the experimental and computational results of the pressure distributions along the square, C3 and C5 cylinders at $\alpha = 0°$ for $Re = 6 \times 10^4$. Right-hand side is an enlarged figure. The ordinate shows the pressure coefficient, and the abscissa shows the angle of the stagnation point θ.

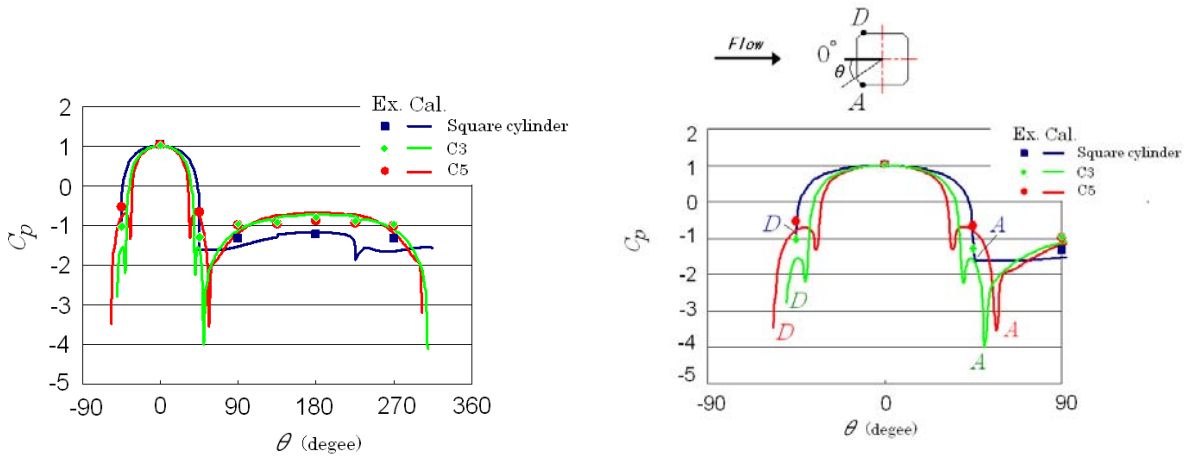

Fig.16. The computational results of the pressure distributions along the cylinder.

The results of the numerical analysis agree well with the experimental values. The pressure coefficient of the square cylinder is a large value, while that of the C3 cylinder is a small value on the part of the front face at about $\theta = -45 \sim +45°$. The pressure coefficient of the square cylinder is a small value, while that of the C3 and C5 cylinders are large values on the part of the side and back face at about $\theta = 90 \sim 270°$, so the drag coefficient of C3 cylinder becomes small.

Figure 17 shows the variations of C_D with the width of the wake for the three kinds of cylinders at $\alpha = 0°$ for $Re = 1 \times 10^3$. The ordinate shows the drag coefficient C_D. The abscissa shows the visualization results of the width of the wake b/d (b is the width of wake, d is the side length of the cross section of the cylinder) at $l/d = 1.5$ behind the cylinders (l is the distance of the central axis of the cylinder to b). It is clear that the drag coefficient becomes large as the width of the wake becomes large at $\alpha = 0°$.

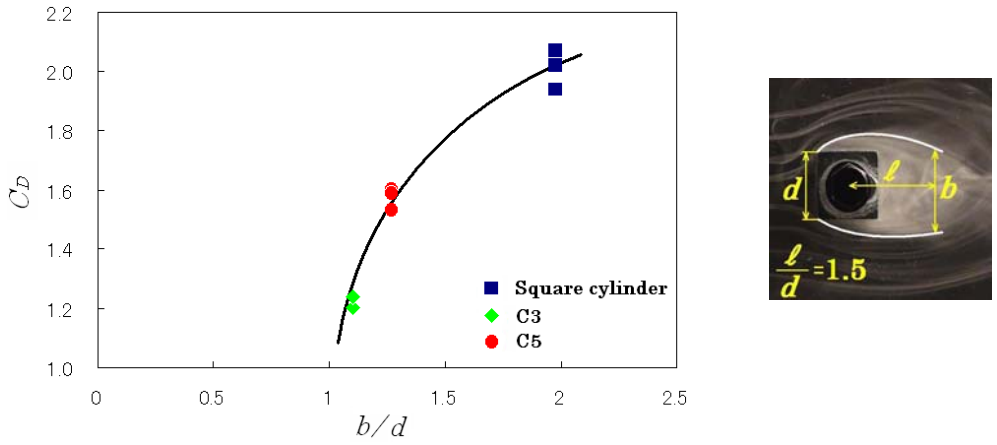

Fig. 17. Drag coefficient with the non dimensional width of wake for cylinders.

Figure 18 shows the variations in the Strouhal number St ($St = fd/U$, f is the frequency of generating vortex, d is the side length of the cross section of the cylinder, and U is the uniform velocity) with an angle of attack α for the cylinders. We found that the drag coefficients of C3 and C5 cylinders become smaller than that of the square cylinder, since the value of the Strouhal numbers of C3 and C5 cylinders become large compared with that of the square cylinder. The Strouhal number of C3 cylinder is the almost same value as C5 cylinder.

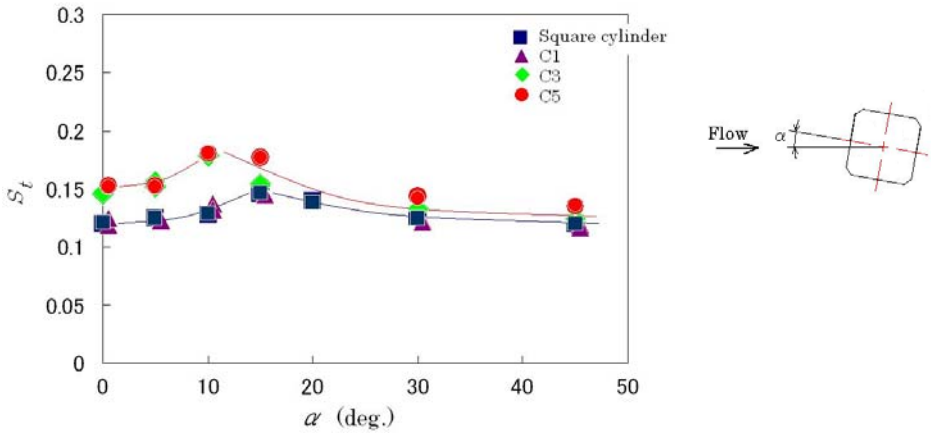

Fig. 18. Relationship between Strouhal number and angle of attack

CONCLUSIONS

The results of the experiments and the numerical analysis around square cylinders with corner cutoffs lead to the following conclusions:

(1) The C3 cylinder is the smallest value of the drag coefficient C_D for square cylinders with changing chamfer shape.

(2) The sudden decrease of the drag coefficient C_D occurs at about an angle of attack α = 0 ~10° in the case of the C3 and C5 cylinders compared with that for the square cylinder. The minimum value of the drag coefficient C_D for the C3 cylinder decreases by about 30% compared with that for the square cylinder.

(3) The value of the drag coefficient C_D of each cylinder for an angle of attack 0° is a constant value of about 2 in the range of C/d = 0 (Square cylinder) ~ 0.033 (C1 cylinder), (C is the chamfer dimension), falls abruptly to a minimum value of about 1.2 at C/d = 0.1 (C3 cylinder), and then increases slightly.

(4) It is clear that the tangential velocity of the corner end side of C5 cylinder becomes large compared with C3 cylinder, and enlarges the separation area of square cylinder side face. Therefore, the width of the wake behind the C3 cylinder becomes small, and then the drag coefficient C_D decreases.

(5) We noted that the drag coefficients C_D of C3 and C5 cylinders become smaller than that of the square cylinder, when the value of Strouhal number of C3 and C5 cylinders become large compared with that of the square cylinder.

REFERENCES

Igarashi, T. (1984), “Characteristics of the Flow around Square Prisms”, Transactions of the Japan Society of Mechanical Engineers, **50**(449), 210-218.

Koide, M., H. Okanaga, and K. Aoki (2006), “Drag reduction Effect of Square Cylinders by Grooves and Corner-cuttings”, Journal of the Visualization Society of Japan, **26**(1), 69-72.

Kurata, M. and T. Morishita (1998), “Drag Reduction of a Bluff Body with Small Cutout at Its Edges”, Transactions of the Japan Society of Mechanical Engineer, **64**(618), 397-404.

Layukallo, T. and Y. Nakamura (2003), “Passive Separation Control on a Square Cylinder at Transonic Speed”, Transactions of the Japan Society for Aeronautical and Space Sciences, **45**(150), 236-242.

Lee, B. E. (1975), “The Effect of Turbulence on the Surface Pressure Field of a Square Prism”, J. Fluid Mech., **69**(2), 263-282.

Ohtsuki, S., K. Fujii, K. Washizu and T. Ohya (1978), Symposium of Japan Association for Wind Engineering, No.5, 169-176.

Shao, C. P., J. M. Wang and Q. D. Wei (2007), “Visualization Study on Suppression of Vortex Shedding from a Cylinder”, Journal of Visualization, **10**(1), 57-64.

Yamagishi, Y., S. Akaike and M. Nemoto (2004), “Effect of the Grooves on Flow Characteristics around a Square Prism”, 52th Symposium of Turbomachinery Society of Japan-Niigata, 118-123.